

Room temperature 2D ferromagnetism in few-layered 1T-CrTe₂

Xingdan Sun,^{1,2,*} Wanying Li,^{1,2,*} Xiao Wang,^{3,4,5,*} Qi Sui,^{6,*} Tongyao Zhang,^{7,8} Zhi Wang,^{1,2} Long Liu,^{1,2} Da Li,^{1,2} Shun Feng,^{1,2,11} Siyu Zhong,⁹ Hanwen Wang,^{1,2} Vincent Bouchiat,¹⁰ Manuel Nunez Regueiro,¹⁰ Nicolas Rougemaille,¹⁰ Johann Coraux,¹⁰ Zhenhua Wang,^{1,2} Baojuan Dong,^{7,8} Xing Wu,⁹ Teng Yang,^{1,2†} Guoqiang Yu,^{3,4,5†} Bingwu Wang,^{6†} Zheng Vitto Han^{1,2,7†} Xiufeng Han,^{3,4,5} Zhidong Zhang^{1,2}

¹Shenyang National Laboratory for Materials Science, Institute of Metal Research,
Chinese Academy of Sciences, Shenyang 110016, China

²School of Material Science and Engineering, University of Science and Technology of China, Anhui 230026, China

³Beijing National Laboratory for Condensed Matter Physics,
Institute of Physics, Chinese Academy of Sciences, Beijing 100190, China

⁴Center of Materials Science and Optoelectronics Engineering,
University of Chinese Academy of Sciences, Beijing 100049, China

⁵Songshan Lake Materials Laboratory, Dongguan, Guangdong 523808, China

⁶Beijing National Laboratory for Molecular Sciences,
Beijing Key Laboratory of Magnetolectric Materials and Devices,

College of Chemistry and Molecular Engineering, Peking University, Beijing, 100871 China

⁷Collaborative Innovation Center of Extreme Optics, Shanxi University, Taiyuan 030006, P.R.China

⁸State Key Laboratory of Quantum Optics and Quantum Optics Devices,
Institute of Opto-Electronics, Shanxi University, Taiyuan 030006, P. R. China

⁹Shanghai Key Laboratory of Multidimensional Information Processing Department of Electrical
Engineering East China Normal University, 500 Dongchuan Road, Shanghai 200241, China

¹⁰University of Grenoble Alpes, CNRS, Institut Néel, F-38000 Grenoble, France. and

¹¹School of physical science and technology, ShanghaiTech University, Shanghai 200031, China.

Spin-related electronics using two dimensional (2D) van der Waals (vdW) materials as a platform are believed to hold great promise for revolutionizing the next generation spintronics. Although many emerging new phenomena have been unravelled in 2D electronic systems with spin long-range orderings, the scarcely reported room temperature magnetic vdW material has thus far hindered the related applications. Here, we show that intrinsic ferromagnetically aligned spin polarization can hold up to 316 K in a metallic phase of 1T-CrTe₂ in the few-layer limit. This room temperature 2D long range spin interaction may be beneficial from an itinerant enhancement. Spin transport measurements indicate an in-plane room temperature negative anisotropic magnetoresistance (AMR) in few-layered CrTe₂, but a sign change in the AMR at lower temperature, with -0.6% at 300 K and +5% at 10 K, respectively. This behavior may originate from the specific spin polarized band structure of CrTe₂. Our findings provide insights into magnetism in few-layered CrTe₂, suggesting potential for future room temperature spintronic applications of such 2D vdW magnets.

Spin-polarized 2D vdW layers have been a cutting-edge topic in recent years, as it not only provides opportunities for new-concept nanostructures,[1–5] but also serves as a test-bed for novel spin physics.[6, 7] Especially, spintronic devices built with vdW magnets have aroused great interest.[8] For example, magnetoresistance in spin-filtered magnetic vdW heterojunctions was manifested to be as high as 10000%, far superior to that of conventionally grown magnetic thin films.[9] More recently, current-induced magnetic switch was succeeded in the Fe₃GeTe₂ few-layers,[10] suggesting vdW magnet a versatile platform for nanoelctronics. However, most of those demonstrated vdW spintronic devices are functioning at low temperature, which are practically not preferable.

Interestingly, even in those vdW magnets with relatively low intrinsic Curie temperature (T_C) such as Fe₃GeTe₂, room temperature 2D ferromagnetism can often be realized via certain extrinsic manners, such as strong electron doping with an ionic gate,[5] or the enhancement of magnetic anisotropic energy through a micrometer-sized geometric confinement.[11] Nevertheless, these methods are in principle incompatible with large scale solid state device applications. Demonstrations of spintronic devices based on intrinsic room temperature ferromagnetic vdW materials remain challenging.

To date, intrinsic vdW ferromagnets with T_C above 300 K have been reported in a very limited library of materials, including epitaxially or chemical vapour/exfoliation synthesized 2D films of MnSe_x[12], VTe₂[13] and VSe₂[14, 15]. Yet it is still plausible about

* These authors contribute equally.

†Corresponding to: yangteng@imr.ac.cn, wangbw@pku.edu.cn, guoqiangyu@iphy.ac.cn, and vitto.han@gmail.com

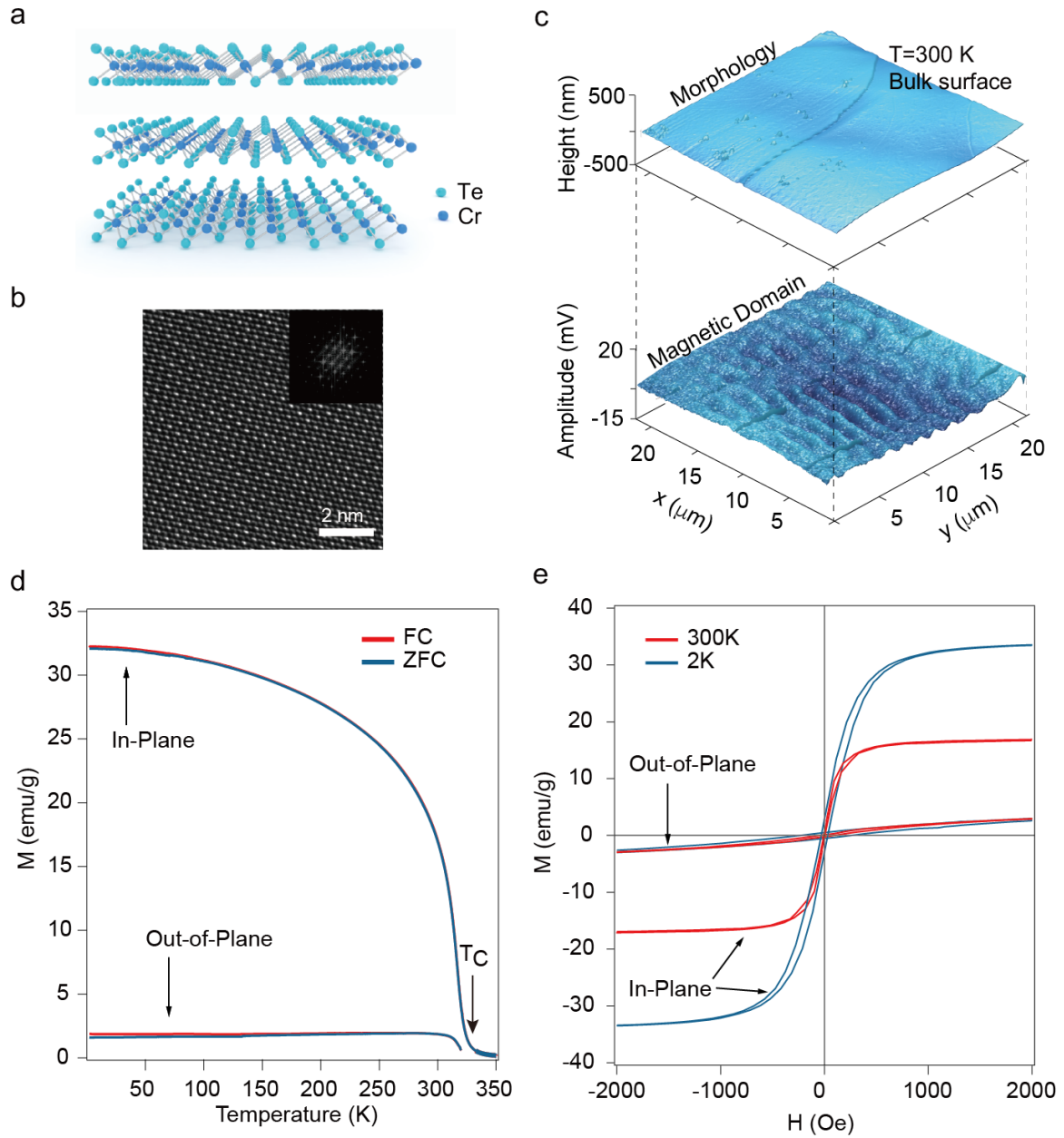


FIG. 1. **Characterizations of bulk 1T-CrTe₂.** (a) Schematics of CrTe₂ crystal structure. (b) Transmission electron micrograph of CrTe₂ crystal. Inset shows the fast Fourier transform pattern of the obtained atomic micrograph. (c) AFM morphology image of a typical CrTe₂ surface freshly exfoliated from a bulk crystal, with its amplitude profile plotted in lower panel, indicating a fringe-like magnetic domain. Images are obtained at room temperature. (d) ZFC-FC curves of bulk CrTe₂. Solid arrow indicates the Curie temperature. (e) Magnetization hysteresis loops of bulk CrTe₂ at 2 K (blue lines) and 300 K (red lines), respectively.

their origin of magnetism since MnSe_x and VTe₂ were reported in absence of an experimentally well defined T_C. [12, 13] The origin of ferromagnetism in the 2D limit in MnSe_x and VSe₂ are yet to be fully understood, as bulk forms of them are known to be non-magnetic. [16–19] Recent theoretical and experimental analysis indicate that a charge density wave phase may be playing key roles in the magnetic order of VSe₂. [20–23] During the

preparation of this manuscript, we notice that bulk vdW Fe₅GeTe₂ has a T_C of about 310 K, while its few-layer samples has T_C of about 270 K, slightly lower than room temperature. [24]

It is noticed that Cr_xTe_y has been one of the overlooked families so far in the hunt for room temperature vdW magnets. Among them, 1T-CrTe₂ is a layered compound with ferromagnetism critical temperature of ~320

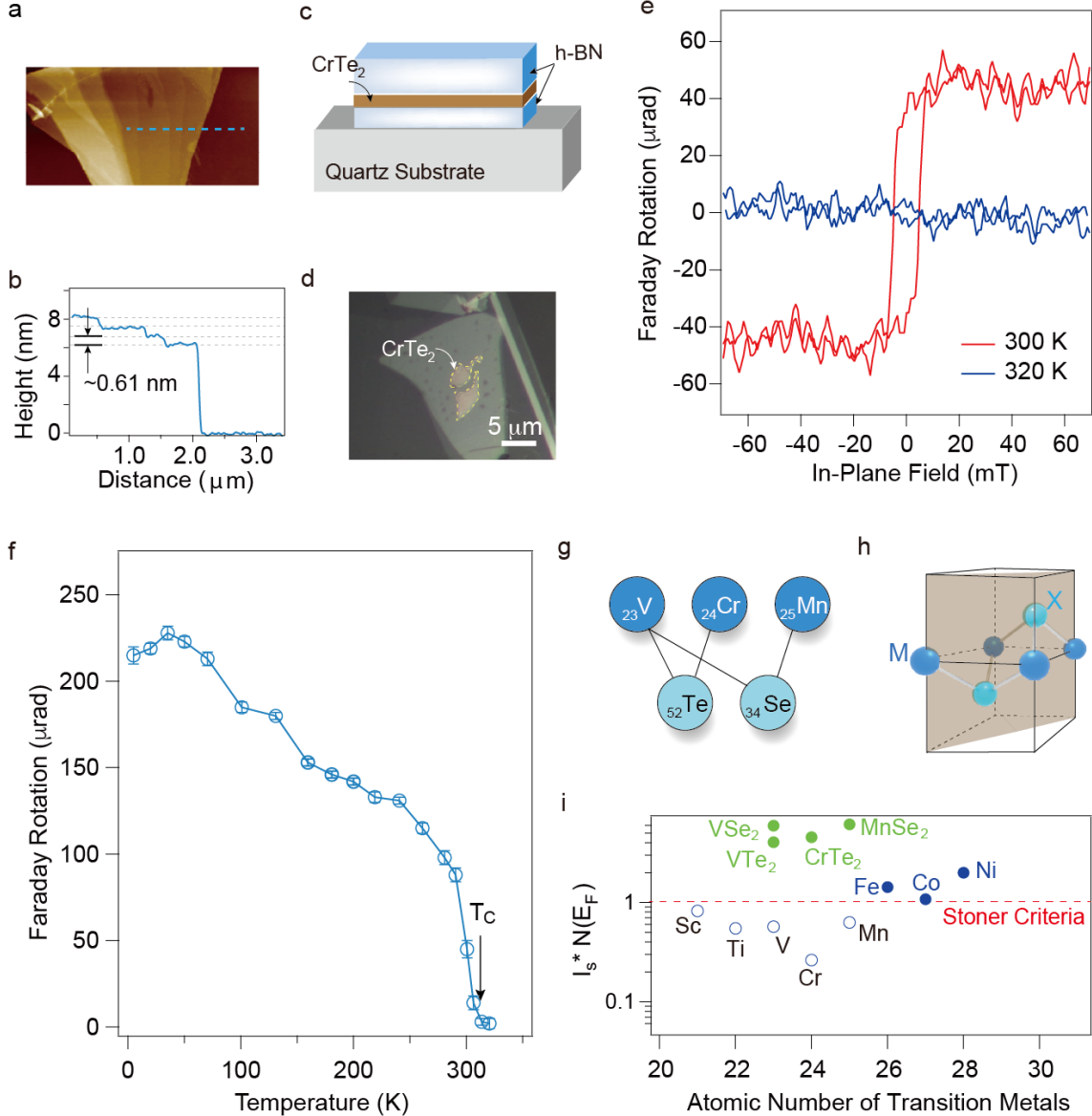


FIG. 2. **Magnetic properties of few-layered CrTe₂.** (a) AFM morphology image of a typical few-layered CrTe₂. (b) Height profile along the dashed line in (a), with the layer thickness measured to be around 0.61 nm, as indicated by the arrows. (c) Schematic picture and (d) optical image of BN-encapsulated few-layered CrTe₂ deposited on a quartz substrate for optical measurements. (e) Faraday rotation of a typical 10 nm CrTe₂ flake at 300 K and 320 K, respectively. (f) M-T curve extracted from the Faraday rotation at 40 mT. (g) A summarization of the four types of known room temperature vdW ferromagnets. (h) Unit cell of MX₂. (i) Analysis of potential band ferromagnetism of several materials using the Stoner criteria.

K in its bulk phase, making it a candidate for the investigation of 2D ferromagnetism.[25] In this work, we performed mechanical exfoliation of a bulk vdW crystal of 1T-CrTe₂, and found that the Curie temperature above 300 K for bulk CrTe₂ can be retained down to the few-layered 2D limit. Our simulations suggest that exchange coupling due to an enhancement of itinerant type was the source of room temperature ferromagnetism in both bulk and few-layered CrTe₂. The 2D ferromagnetism in few-

layered CrTe₂ was further investigated in the framework of in-plane AMR at different temperatures. Our findings demonstrate that few-layered CrTe₂ can be a candidate for next generation room temperature spin-related 2D nanoelectronics.

RESULTS

Characterizations of bulk phase of CrTe₂. Bulk CrTe₂ single crystals were prepared (see Methods) and were confirmed via x-ray diffraction (Supplementary Figure 1). It is known that 1T-CrTe₂ has a layered structure with lattice symmetry of space group $P\bar{3}m1$ (Fig. 1a). To confirm the crystalline structure of the as-synthesized crystals, we performed transmission electron micrograph (TEM) of an exfoliated CrTe₂ flake, as shown in Fig. 1b. Clear hexagonal lattice structure, resembling the top view of Fig. 1a, can be seen. Atomic force microscopy was used to characterize the morphology (upper panel of Fig. 1c) with its corresponding magnetic domain shown in the lower panel of Fig. 1c. As can be seen, at room temperature, the bulk CrTe₂ has a fringe-like magnetic domain, with the domain width of about $1 \sim \mu\text{m}$. Zero-field-cooled (ZFC) and field-cooled (FC) thermal magnetization curves of bulk CrTe₂ were obtained. As shown in Fig. 1d, the Curie temperature T_C is determined to be around 320 K with a 1,000 Gauss magnetic field applied. To clarify the magnetization behavior of bulk CrTe₂, M-H loops were examined at 10 K and 300 K, which are both typically ferromagnetic, as shown in Fig. 1e.

Magnetic properties of exfoliated few-layered CrTe₂. In order to study the magnetism of CrTe₂ in the 2D limit, we carried out mechanical exfoliation using the standard scotch tape method.[26] Atomic Force Microscope (AFM) scan of a typical CrTe₂ flake (thinnest part of ~ 6.1 nm) is shown in Fig. 2a-b. It is found that the yield of atomically thin CrTe₂ is rather low compared to those easily exfoliated layered compound such as graphene, and the thinnest flake we could obtain was ~ 3 nm (Supplementary Figure 2). Moreover, similar to other telluride materials, few-layered CrTe₂ in air is easily degraded, leading to failure for any further characterizations (Supplementary Fig. 3). Hexagonal boron nitride (h-BN) encapsulation in a glove box therefore can be a solution to avoid air-degradation of ultra-thin CrTe₂ flakes. A detailed Raman spectra measurements of few-layered CrTe₂ is given in Supplementary Figures 4-6. It is found that intrinsic thin flakes of CrTe₂ show Raman shift peaks at about 99.7 and 132 cm^{-1} , while degraded ones will shift its characteristic peaks to 120 and 140 cm^{-1} with higher intensity. It thus provides us a quick way to select the pristine thin flakes for magnetic and electrical measurements.

With protection from air, the h-BN sandwiched thin layers of CrTe₂ were deposited onto transparent quartz substrates for Faraday measurements, as sketched in Fig. 2c. Oblique incident probe beam with respect to the sample plane was applied to monitor the in-plane component of the magnetization in the few-layered CrTe₂ flakes (Supplementary Figure 7). Spot size of about 2 μm diameter laser with wavelength of 800 nm was used,

and an optical image of typical sample is shown in Fig. 2d. A typical 10 nm CrTe₂ sample was loaded in a vacuum chamber and measured in a transmission configuration (Supplementary Figure 7) with its magnetization hysteresis loops (M-H loops). As shown in Fig. 2e, the few-layered CrTe₂ exhibits characteristic ferromagnetic M-H loops at 300 K, while the loop became a linear background above 320 K. We extracted the saturated Faraday effect signal at $H=40$ mT, and thus obtained an effective M-T curve, shown in Fig. 2f. The general trend of M-T in few-layered CrTe₂ is rather similar to that measured in its bulk, with a T_C to be around 316 K in few-layered CrTe₂, as indicated by the solid arrow in Fig. 2f.

Interestingly, among the known room temperature 2D ferromagnets, i.e., VSe₂, MnTe₂, MnSe_x, and CrTe₂, they all belong to a family of transitional metal dichalcogenides MX₂ with octahedral units (1T), as illustrated in the cartoon in Fig. 2g-2h. The triangle M sublattice of the 1T major phase gives rise to a first-neighbor coordination number of 6. Besides the indirect superexchange coupling, itinerant exchange [27] should be playing an essential role due to the metallic nature of these room temperature vdW ferromagnets. To test whether itinerant (or band) ferromagnetism appears in a metal, one usually refers to the so-called Stoner criteria, namely the $I_s * N(E_F) \geq 1$ condition [28]. The I_s quantity is called Stoner exchange integral, which depends very little on bonding environments [28], and $N(E_F)$ is the electronic density of states at the Fermi level. In Fig. 2i, four typical MX₂ 2D room temperature ferromagnets are given, and compared to both the corresponding elemental metals and ferromagnetic Fe, Co and Ni elemental metals. Expectedly, only Fe, Co and Ni among all the given elemental metals meet the Stoner criteria to exhibit band ferromagnetism. However, the 2D VSe₂, CrTe₂, MnTe₂ and MnSe₂ have $I_s * N(E_F)$ much increased upon that of the corresponding elementary metals, and the Stoner criteria is then met for a band ferromagnetism in these 2D materials. The chalcogenide atoms are important in boosting ferromagnetism in terms of the following: (i) Double superexchange. Neighbouring magnetic elements M (= V, Cr, Mn) are coupled to each other by superexchange through M-X-M bonds of nearly 90° bond angle. (ii) Enhancement of $N(E_F)$. Electronic density of states (DOS) at Fermi level of MX₂ is enhanced upon $N(E_F)$ of the corresponding elemental metals, due to orbital rearrangement by the X atoms. The partial DOS analysis shows that $N(E_F)$ in 1T-MX₂ is overwhelmingly from the orbitals of M atoms (Supplementary Figure 8). (iii) The Slater criterion [29]. In this criterion, a ratio $\frac{r}{2r_a}$ of interatomic distance r over the double atomic radius $2r_a$ has to exceed 1.5 for the occurrence of ferromagnetism [29, 30], with Fe, Co and Ni elementary metals satisfying this criterion, while V, Cr and Mn not. The existence of chalcogenide X atoms in those 2D 1T-MX₂ may play a role in enlarging the interatomic separation

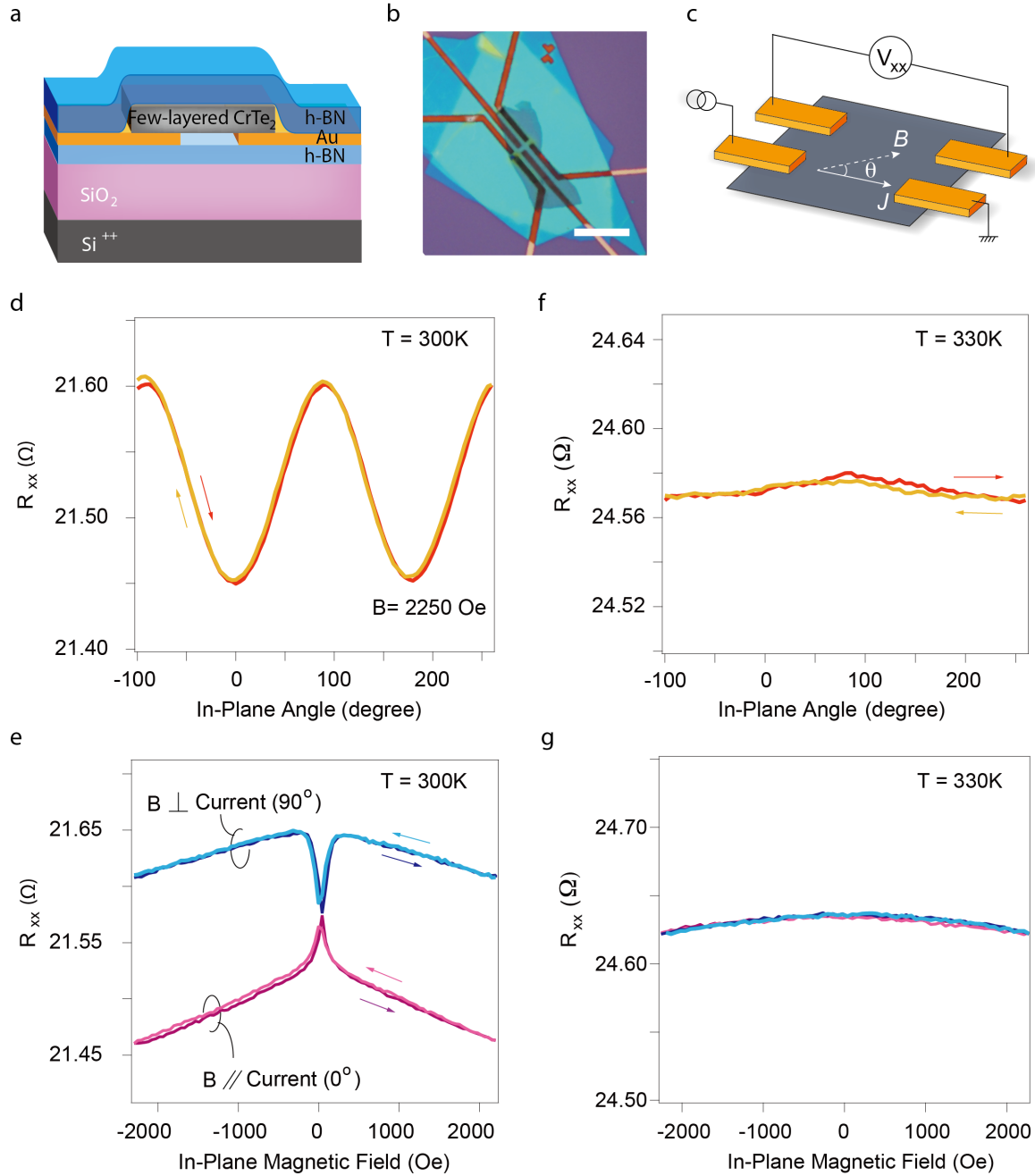


FIG. 3. **Anisotropic magnetoresistance of few-layered CrTe₂ at 300 K.** (a) Art view and (b) Optical image of a typical h-BN/CrTe₂/h-BN device. Scale bar in (b) is 10 μm . (c) Illustration of the measurement of in-plane magnetic field with an angle θ against the current \mathbf{J} . (d) R_{xx} of few-layered CrTe₂ as a function of θ with an 2250 Oe magnetic field applied. (e) R_{xx} of few-layered CrTe₂ as a function of magnetic field \mathbf{B} , with $\theta=0^\circ$ (pink lines) and 90° (blue lines), respectively. (f) and (g) are R_{xx} vs θ , and R_{xx} vs \mathbf{B} with the same configurations as in (d)-(e) measured at 330 K.

of V, Cr and Mn, so as to meet the Slater criterion.

To further quantify the strength of itinerant exchange interaction, mean-field solution to the Heisenberg model is employed [28, 31], namely, $T_c = \frac{2zJS(S+1)}{3k_B}$, in which z is the coordination number (for instance $z = 6$ in 1T MX₂), J is the exchange, and S is the spin angular momentum (orbital angular momentum $L = 0$ due to orbital

quenching in octahedral MX₂). We therefore evaluate the exchange J in terms of $J = \frac{3k_B T_c}{2zS(S+1)}$ and show it in Supplementary Figure 9. The exchange strength J , around 70-120 meV , is comparable to that in the elemental ferromagnets and 2D itinerant ferromagnets, but much larger than that in non-itinerant 2D magnets such as CrI₃ (Supplementary Figure 9). We have to admit

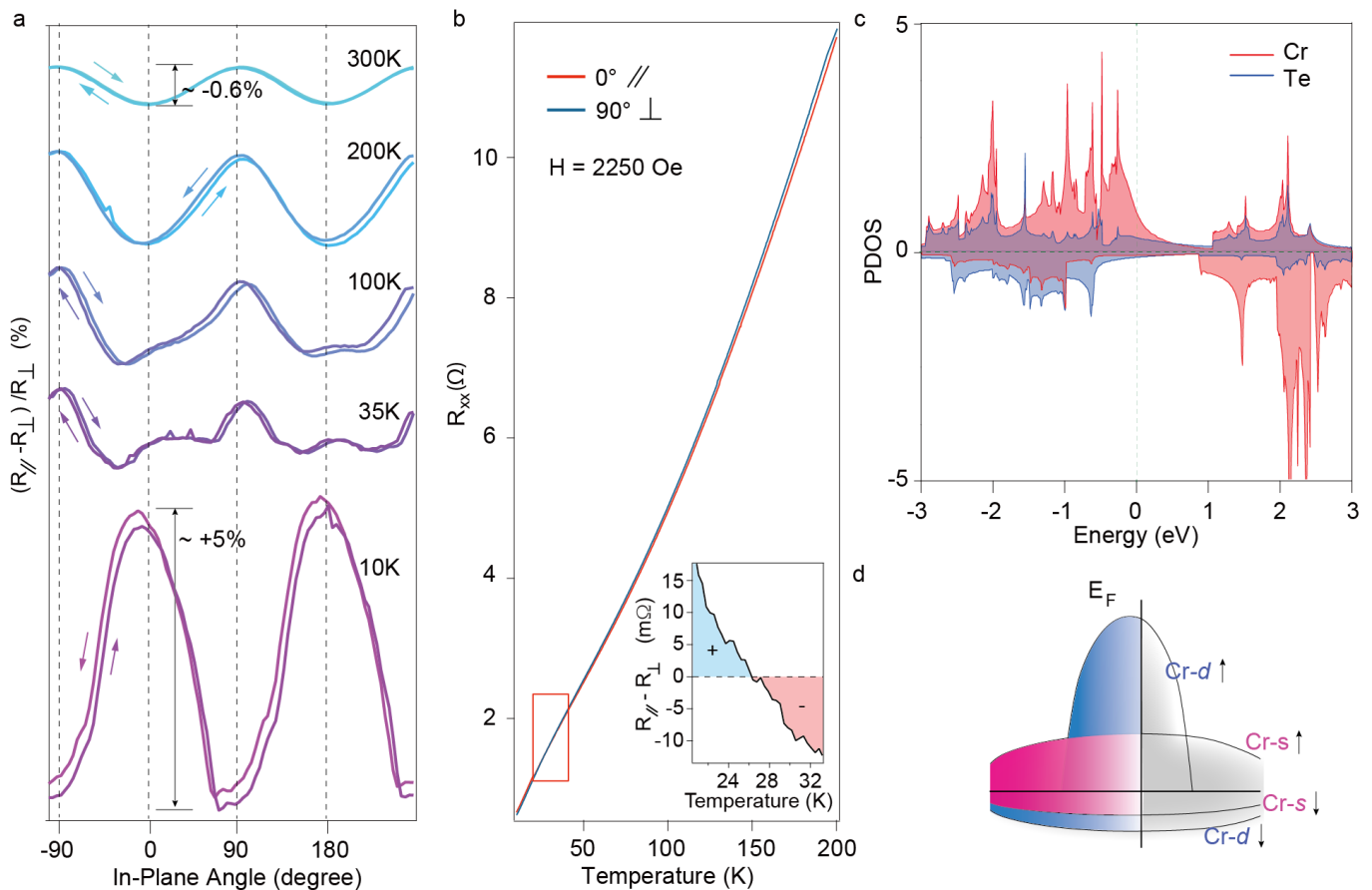


FIG. 4. **Mechanism of AMR in few-layered CrTe₂.** (a) r_{AMR} of few-layered CrTe₂ at different temperatures. (b) R_{xx} as a function of temperature at $\theta=0^\circ$ (red line) and 90° (blue line). An in-plane magnetic field of 2250 Oe was applied. Inset shows the difference between R_{\parallel} and R_{\perp} , with negative and positive values separated at the temperature of about 26.5 K. (c) Partial DOS (PDOS) from both Cr and Te for spin up and spin down sub bands calculated for monolayer CrTe₂. (d) Schematic image of the decomposed Cr-s and Cr-d orbitals near the Fermi level.

that the evaluation of exchange is more or less simplified due to the lack of consideration of several factors including magnetocrystalline anisotropy, and the exceptional cases of charge density wave (CDW) in VSe₂ and VTe₂ [32, 33]. A thorough understanding on the room temperature ferromagnetism in the 2D 1T-MX₂ remains an open question.

DISCUSSION

Spin transport of CrTe₂ in the 2D limit. We now come to the investigation of spin transport behaviour in few-layered CrTe₂. Different ways of protection methods were performed, including Pt thin film capping and BN-encapsulation (Supplementary Figures 10-11), in order to enhance the air-stability of few-layered CrTe₂. In general, ultra thin CrTe₂ can be quite stable as long as heating is well avoided during the whole fabrication process. As sketched in Fig. 3a, the CrTe₂ flakes were encapsulated by two h-BN flakes, with Au electrodes patterned

in between via lithography. Optical image of a typical BN-encapsulated device is shown in Fig. 3b. Because of the in-plane magnetic anisotropy, no detectable Hall signal was obtained in those devices. In the following, we mainly focus on the longitudinal resistance R_{xx} , with the configuration for measurements illustrated in Fig. 3c.

Fig. 3d shows R_{xx} at 2250 Oe, recorded in a typical CrTe₂ device with thickness of 10 nm, as a function of the angle θ between the in-plane magnetic field \mathbf{B} and the electrical current \mathbf{J} flowing between source and drain electrodes. A two-fold $\cos(2\theta)$ -like oscillation behaviour was observed, similar to previously reported.[34, 35] Fig. 3e shows the corresponding magnetoresistance (M-H curves) at 300 K for $\theta=0^\circ$, and 90° , respectively (data at more temperatures shown in Supplementary Figure 12). It is noted that when heated up to 330 K, the AMR related features disappear, and can be re-appearing once the sample is cooled back down to 300 K. This is a prove that the ferromagnetic-paramagnetic phase transition in few-layered CrTe₂ is reversible. This observed negative in-plane AMR behaviour (reproduced in multiple sam-

ples as shown in the Supplementary Figures 13) is seen in some conventional half-metallic ferromagnets such as Ni_3FeN [34], as well as in recently reported Mn-doped Bi_2Se_3 [36]. On the contrary, many other ferromagnets, such as Ni and Fe,[37] and vdW materials Fe_3GeTe_2 [38] (with much smaller r_{AMR}) have positive in-plane AMR.

When further cooled down, as shown in Fig. 4a, the shape of r_{AMR} became more or less deviated from the $\cos(2\theta)$ symmetry. At 10 K, the general r_{AMR} changes its sign from negative into positive, with its amplitude reaching 5%, at the same order of magnitude as compared the maximum AMR reported in the NiFe alloys [39, 40]. However, NiFe alloys such as Ni_3FeN thin film has positive r_{AMR} at room temperature and negative r_{AMR} at low temperature [34], which are quite opposite with respect to that observed in few-layered CrTe_2 . According to the spin scattering model [41] $r_{\text{AMR}} = \frac{R_{\parallel} - R_{\perp}}{R_{\perp}} \propto -(N_{\uparrow}^d - N_{\downarrow}^d) \cdot (\sigma_{\uparrow} - \sigma_{\downarrow})$, the competition between conducting electrons at each spin branch will be the origin of the sign change on the experimentally obtained r_{AMR} at different temperatures.

We recorded the R-T curves of R_{xx} for the same device measured in Fig. 4a, at $\theta=0^\circ$ (red solid line) and 90° (blue solid line), with a fixed in-plane magnetic field of 2250 Oe, as shown in Fig. 4b. A crossing point can be seen in the boxed area, as also zoomed in the inset, at the temperature of about 26.5 K. By computing the partial density of states (PDOS) of mono-layer CrTe_2 , it is clearly seen in Fig. 4c and Supplementary Figure 14 that N_{\uparrow}^d is much larger than N_{\downarrow}^d . Nevertheless, as illustrated in Fig. 4d (more details refer to Supplementary Figure 14), at the Fermi level, the spin majority (\uparrow) Cr d orbital is more localized than the spin minority (\downarrow) Cr d orbital, meanwhile, Cr s orbitals for both spin majority and minority are delocalized. It is therefore expected that spin up electrons contribute to the minority of conductivity, due to a much larger magnitude of s - d scattering in spin up channel than in spin down channel, making $\sigma_{\uparrow} - \sigma_{\downarrow} < 0$, thus a positive r_{AMR} at low temperature. When thermal excitation takes over with increasing temperature, more spin up Cr d orbitals are occupied, suppressing s - d scattering and giving rise to a sign change in the $\sigma_{\uparrow} - \sigma_{\downarrow}$ term, thus a negative r_{AMR} up to 300 K.

In conclusion, after the three reported room temperature 2D ferromagnets, we have found the 4th one, i.e., CrTe_2 . By optical and electrical measurements, ferromagnetism was proven to be prevailing in CrTe_2 in the few-layered limit, with Curie temperature above 300 K. Detailed spin transport measurements suggest that a half-metallicity in its spin-polarized band structure gives rise to a -0.6 % r_{AMR} at 300 K, which changes into a +5 % r_{AMR} at 10 K. Our studies reveal that vdW 2D ferromagnet CrTe_2 can be a candidate for future room temperature spintronic applications, since it can be, in

principle, further implemented into in-plane spin valves, as well as large size flexible spin devices.

METHODS

The 1T- CrTe_2 single crystals were synthesized indirectly by oxidation of KCrTe_2 . The parent compound KCrTe_2 was prepared by a molar mixture of the corresponding elements (nK:nCr:nTe=1:1:2) under argon atmosphere. The mixture was heated at 900 °C for seven days in an evacuated quartz tube and then cooled to room temperature at the rate of 10 °C h⁻¹. The as-synthesized black parent compound KCrTe_2 was dispersed in acetonitrile and the excess iodine was added very slowly. After stirring for 12 hours, the residue was washed with acetonitrile for three times and the brilliant dark gray platelets 1T- CrTe_2 were obtained. The h-BN (crystals from HQ Graphene) encapsulated CrTe_2 devices were fabricated using the dry-transfer methods (Supplementary Figures 31)[3] in a glove box. A Bruker Dimension Icon AFM was used for thicknesses and morphology tests. Raman measurements were performed by an HR 800 JobinYvon Horiba polarized Raman spectroscopy. The electrical performances of the devices were measured using a physical properties measurement system (PPMS, Quantum Design) and a probe station (Cascade Microtech Inc. EPS150) under ambient conditions.

The electronic properties in this work were calculated by using the first-principles density functional theory as implemented in the VASP code[42]. The electron-ion interaction and electronic exchange-correlation interaction were respectively described by Projector augmented wave (PAW) pseudopotentials [43] and the Perdew-Burke-Ernzerhof (PBE) [44] functional. The electronic kinetic energy cutoff for plane-wave basis was set to be 520 eV. The energy criterion for reaching self-consistency was set to be 10⁻⁸ eV. The Brillouin zones were sampled using the Γ -centered Monkhorst-Pack mesh by 20×20×1 k-points and 40×40×1 k-points for self-consistency and electronic density of states, respectively. [45]

DATA AVAILABILITY

The data that support the findings of this study are available from the corresponding authors upon reasonable request.

ACKNOWLEDGEMENT

This work is supported by the National Key R&D Program of China (2017YFA0206302 & 2017YFA0206200) and the National Natural Science Foundation of China (NSFC) with Grants 11974357, U1932151, and 51627801.

G.Y. and X.H. thank the final supports from the National NSFC with Grant No.11874409. T.Yang acknowledges supports from the Major Program of Aerospace Advanced Manufacturing Technology Research Foundation NSFC and CASC, China (No. U1537204). Z. Han acknowledges the support from the Program of State Key Laboratory of Quantum Optics and Quantum Optics Devices (No. KF201816).

AUTHOR CONTRIBUTIONS

Z.H., B.W., G.Y., T.Y., and Z.Z. conceived the experiment and supervised the overall project. X.S. and W.L. fabricated the devices; X.W.(Xiao Wang), X.S., W.L., D.L., X.H., and G.Y. carried out measurements of spin transport. S.F. performed Raman measurements. T.Z. carried out Faraday rotation measurements; B.D. and T.Y. conducted the theoretical simulations. B.W., Q.S., B.V., C.J., N.R., and M.R. fabricated bulk crystals and performed characterizations of bulk magnetic properties. S.Z. and X.W.(Xing Wu) carried out TEM experiments. L.L. contributed in Pt sputtering. Z.W. discussed on the manuscript. The manuscript was written by Z.H. and X.S. with discussion and inputs from all authors.

ADDITIONAL INFORMATION

Competing interests: The authors declare no competing financial interests.

-
- [1] Huang, B. *et al.* Layer-dependent ferromagnetism in a van der waals crystal down to the monolayer limit. *Nature* **546**, 270–273 (2017).
- [2] Gong, C. *et al.* Discovery of intrinsic ferromagnetism in two-dimensional van der waals crystals. *Nature* **546**, 265 (2017).
- [3] Wang, Z. *et al.* Electric-field control of magnetism in a few-layered van der waals ferromagnetic semiconductor. *Nature Nanotechnology* **13**, 554–559 (2018).
- [4] Jiang, S. W., Shan, J. & Mak, K. F. Electric-field switching of two-dimensional van der waals magnets. *Nature Materials* **17**, 406–410 (2018).
- [5] Yu, Y. J. *et al.* Gate-tunable room-temperature ferromagnetism in two-dimensional Fe₃GeTe₂. *Nature* **563**, 94–99 (2018).
- [6] Sun, Z. Y. *et al.* Giant nonreciprocal second-harmonic generation from antiferromagnetic bilayer CrI₃. *Nature* **572**, 497–501 (2019).
- [7] Chen, W. J. *et al.* Direct observation of van der waals stacking dependent interlayer magnetism. *arXiv* 1906.03383 (2019).
- [8] Li, X. *et al.* Perspectives on exfoliated two-dimensional spintronics. *Journal of Semiconductors* **40**, 081508 (2019).
- [9] Song, T. C. *et al.* Giant tunneling magnetoresistance in spin-filter van der waals heterostructures. *Science* **360**, 1214–1218 (2018).
- [10] Wang, X. *et al.* Current-driven magnetization switching in a van der waals ferromagnet Fe₃GeTe₂. *Science Advances* **5** (2019).
- [11] Li, Q. *et al.* Patterning-induced ferromagnetism of Fe₃GeTe₂ van der waals materials beyond room temperature. *Nano Lett.* **18**, 5974–5980 (2018).
- [12] OHara, D. J. *et al.* Room temperature intrinsic ferromagnetism in epitaxial manganese selenide films in the monolayer limit. *Nano Letters* **18**, 3125–3131 (2018).
- [13] Li, J. *et al.* Synthesis of ultrathin metallic MTe₂ (M = V, Nb, Ta) single-crystalline nanoplates. *Advanced Materials* **30**, 1801043 (2018).
- [14] Yu, W. *et al.* Chemically exfoliated VSe₂ monolayers with room-temperature ferromagnetism. *Advanced Materials* 1903779 (2019).
- [15] Bonilla, M. *et al.* Strong room-temperature ferromagnetism in VSe₂ monolayers on van der waals substrates. *Nature Nanotechnology* **13**, 289–293 (2018).
- [16] Onari, S. & Arai, T. J. Infrared lattice vibrations and dielectric dispersion in antiferromagnetic semiconductor MnSe₂. *Phys. Soc. Jpn.* **46**, 184188 (1979).
- [17] Pollard, R. J., McCann, V. H. & Ward, J. B. Magnetic structures of α -MnS and MnSe from ⁵⁷Fe mossbauer spectroscopy. *J. Phys. C: Solid State* **16**, 345 (1983).
- [18] van Bruggen, C. F. & Haas, C. Magnetic susceptibility and electrical properties of VSe₂ single crystals. *Solid State Commun.* **20**, 251254 (1976).
- [19] Bayard, M. & Sienko, M. J. Anomalous electric and magnetic properties of vanadium diselenide. *J. Solid State Chem.* **19**, 325329 (1976).
- [20] Liu, H. *et al.* Quasi-2d transport and weak antilocalization effect in few-layered VSe₂. *Nano Letters* **19**, 4551–4559 (2019).
- [21] Jolie, W. *et al.* Charge density wave phase of VSe₂ revisited. *Phys. Rev. B* **99**, 115417 (2019).
- [22] Chen, P. *et al.* Unique gap structure and symmetry of the charge density wave in single-layer VSe₂. *Phys. Rev. Lett.* **121**, 196402 (2018).
- [23] Feng, J. G. *et al.* Electronic structure and enhanced charge-density wave order of monolayer WSe₂. *Nano Lett.* **18**, 4493–4499 (2018).
- [24] May, A. F. *et al.* Ferromagnetism near room temperature in the cleavable van der waals crystal Fe₅GeTe₂. *ACS Nano* **13**, 44364442 (2019).
- [25] Freitas, D. C. *et al.* Ferromagnetism in layered metastable 1T-CrTe₂. *Journal of Physics: Condensed Matter* **27**, 176002 (2015).
- [26] Novoselov, K. S. *et al.* Electric field effect in atomically thin carbon films. *Science* **306**, 666–669 (2004).
- [27] Stoner, E. Collective electron specific heat and spin paramagnetism in metals. *Proc. Roy. Soc. A* **154**, 656 (1936).
- [28] Mohn, P. *Magnetism in the Solid State* (Springer-Verlag, Berlin, 2003).
- [29] Slater, J. C. Atomic shielding constants. *Phys. Rev.* **36**, 57–64 (1930).
- [30] Omar, M. A. *Elementary Solid State Physics: Principles and applications* (Addison-Wesley Publishing Company, Inc., 2001).
- [31] Blundell, S. *Magnetism in condensed matter* (Oxford University Press, Great Clarendon Street, Oxford OX2 6DP, UK, 2001).

- [32] Sugawara, K. *et al.* Monolayer VTe₂: Incommensurate fermi surface nesting and suppression of charge density waves. *Phys. Rev. B* **99**, 241404 (2019). URL <https://link.aps.org/doi/10.1103/PhysRevB.99.241404>.
- [33] Yu, W. *et al.* Chemically exfoliated VSe₂ monolayers with room-temperature ferromagnetism. *Advanced Materials* 1903779 (2019).
- [34] Takata, F., Kabara, K., Ito, K., Tsunoda, M. & Suemasu, T. Negative anisotropic magnetoresistance resulting from minority spin transport in Ni_xFe_{4-x}N (x=1 and 3) epitaxial films. *Journal of Applied Physics* **121**, 023903 (2017).
- [35] Tsunoda, M. *et al.* Negative anisotropic magnetoresistance in Fe₄N film. *Applied Physics Express* **2**, 083001 (2009).
- [36] Zhang, D. *et al.* Interplay between ferromagnetism, surface states, and quantum corrections in a magnetically doped topological insulator. *Phys. Rev. B* **86**, 205127 (2012).
- [37] McGuire, T., Aboaf, J. & Klokholm, E. Negative anisotropic magnetoresistance in 3d metals and alloys containing iridium. *IEEE Transactions on Magnetics* **20**, 972–974 (1984).
- [38] You, Y. R. *et al.* Planar topological hall effect in a uniaxial van der waals ferromagnet Fe₃GeTe₂. *arXiv* 1907.02397 (2019).
- [39] Van Elst, H. C. The anisotropy in the magneto-resistance of some nickel alloys. *Physica* **25**, 708–720 (1959).
- [40] Bozorth, R. M. Magnetoresistance and domain theory of iron-nickel alloys. *Phys. Rev.* **70**, 923–932 (1946).
- [41] Kokado, S., Tsunoda, M., Harigaya, K. & Sakuma, A. Anisotropic magnetoresistance effects in Fe, Co, Ni, Fe₄N, and half-metallic ferromagnet: A systematic analysis. *Journal of the Physical Society of Japan* **81**, 024705 (2012).
- [42] Kresse, G. & Furthmüller, J. Efficient iterative schemes for *ab initio* total-energy calculations using a plane-wave basis set. *Phys. Rev. B* **54**, 11169–11186 (1996).
- [43] Kresse, G. & Joubert, D. From ultrasoft pseudopotentials to the projector augmented-wave method. *Phys. Rev. B* **59**, 1758–1775 (1999). URL <http://link.aps.org/doi/10.1103/PhysRevB.59.1758>.
- [44] Perdew, J. P., Burke, K. & Ernzerhof, M. Generalized gradient approximation made simple. *Phys. Rev. Lett.* **77**, 3865–3868 (1996). URL <http://link.aps.org/doi/10.1103/PhysRevLett.77.3865>.
- [45] Monkhorst, H. J. & Pack, J. D. Special points for brillouin-zone integrations. *Phys. Rev. B* **13**, 5188–5192 (1976).